Numerical Simulation of Bubble Growth in a Limited Amount of Liquid

Xingming Xu, Guoqun Zhao, Huiping Li

Engineering Research Center for Mold & Die Technologies, Shandong University, Jinan, Shandong 250061, China

Received 25 March 2009; accepted 18 September 2009
DOI 10.1002/app.31450
Published online 23 December 2009 in Wiley InterScience (www.interscience.wiley.com).

ABSTRACT: In this study, we examined the growth of a spherical bubble in a limited amount of liquid by using a finite-element-based numerical simulation method. The bubble growth was assumed to be controlled by both momentum and mass transfer. A truncated power-law constitutive equation was used to describe the rheology of the melt. The gas inside the bubble followed the ideal gas law. The gas concentration at the bubble surface obeyed Henry's law. A computer code was programmed to solve the equations with the Galerkin method. A backward Euler scheme was used to discretize time. Grids were remeshed after each incremental time step to ensure the accuracy of the numerical results. The bubble growth process was simulated with the code. The numerical results, such as the instantaneous bubble size, gas pressure inside the bubble, and gas concentration profile in the liquid, were predicted. The influences of the liquid volume, initial gas pressure, temperature, and rheology of the melt on bubble growth were also studied. The results of the bubble growth simulation in this study were in satisfactory agreement with others' work. © 2009 Wiley Periodicals, Inc. J Appl Polym Sci 116: 1264–1271, 2010

Key words: diffusion; growth; modeling; rheology; simulations

INTRODUCTION

Polymeric foams appear in diverse fields, such as boiling, vaporization, polymer processing, composite materials, and glass refining, because of their low weight, high strength-to-weight ratios, and sound- and shock-absorbing properties.[1–4] Foams are formed mainly in two different ways: chemical foaming and physical foaming.[5] In the chemical foaming process, bubbles are formed because of a chemical reaction, during which a chemical blowing agent decomposes and releases gas at certain temperature and pressure. In the physical foaming process, a physical blowing agent is injected into the polymer under high pressure, and with the pressure release, the solution becomes supersaturated. At the same time, nucleation and bubble growth begin.[6,7]

There are articles describing the dynamics of diffusion-induced bubble growth and studying the effects of different materials and process parameters on the bubble growth rate, gas pressure inside the bubble (P_g), and bubble size distribution. The researchers in these studies simulated bubble growth in infinite liquids[8–10] and described gas concentration profiles in liquids in the form of polynomials.[11–13] Amon and Denson[14] first introduced the idea of a cell model to analyze bubble growth in limited liquid. Favelukis[13] studied bubble growth in a limited amount of liquid with the cell model. Feng[15] compared the process of bubble growth in infinite and finite liquids. Furthermore, he predicted the cell size distribution. Among the numerical methods, the finite difference method and integral method have been widely used in many studies on bubble growth, and the finite element method was introduced to simulate the bubble growth process gradually in recent years.[11,12,14–19]

Recent articles on bubble growth simulation either describe the dissolved gas concentration distribution in the form of a polynomial or simulated bubble growth in an infinite volume of melt.[12,15] Also, only in a few articles, has the finite element method been used. However, it is a unrealistic to assume that a bubble grows in infinite volume of melt and that the dissolved gas concentration in the melt obeys a polynomial distribution. In this study, a cell model was used to simulate bubble growth in a limited amount of power-law liquid. The finite element method was used to solve the equations with the Galerkin method. We solved the diffusion equation directly to obtain the real concentration of dissolved gas in the melt instead of assuming a polynomial distribution of dissolved gas concentration. The finite element nodes moved with the fluid. Grids were remeshed after each incremental time step. The effect of the rheological characteristics on bubble growth was investigated in detail. The effects of other controlling parameters, such as the amount of melt around the

Correspondence to: G. Zhao (zhaogq@sdu.edu.cn).

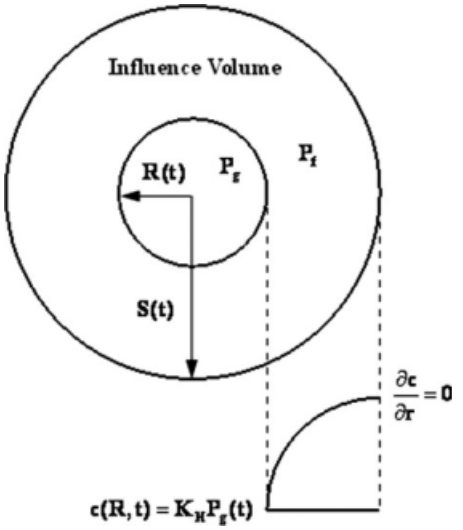

Figure 1 Schematic diagram of a cell model.

bubble, P_g, and polymer temperature on bubble growth, were also studied. The numerical results were more realistic, and the method in this article is suitable to simulate bubble growth.

MODEL DESCRIPTION AND ASSUMPTIONS

Consider a polymer melt with a dissolved gas concentration in equilibrium state with the gas under a gas loading pressure (P_{g0}) inside the bubble. At time $t = 0$, the pressure of the melt drops to ambient pressure dramatically, and the solution becomes supersaturated. At the same time, nucleation and bubble growth begin. P_g and the dissolved gas concentration at the bubble surface decrease as the bubble grows. Figure 1 shows a schematic diagram of bubble growth. $R(t)$, $S(t)$, $c(R,t)$, and $P_g(t)$ represent the bubble radius, outer radius of the cell, gas concentration at the bubble surface, and gas pressure inside the bubble at any time t, respectively, and P_g, P_f, K_H, c, and r represent the gas pressure inside the bubble, ambient pressure, Henry's law constant, dissolved gas concentration in the melt, and distance from any point to the origin of coordinates. The following assumptions were used to analyze the bubble growth process:[12,20,21]

1. The bubble is spherically symmetric because it nucleates until the growth finishes.
2. The gas concentration distribution is uniform throughout the melt before bubble growth, and the gas concentration at the bubble surface obeys Henry's law as shown in eq. (1):

$$c(R,t) = K_H P_g(t) \tag{1}$$

3. The gas in the bubble follows the ideal gas law, and there is no loss of gas to the surroundings.
4. The material properties remain constant during the period of bubble growth, and the melt is assumed to be incompressible.
5. The effect of gravity is neglected because of the high viscosity of the polymer melt.
6. The growth process is considered isothermal as the timescale of bubble growth is sufficiently small and is much smaller than that of the cooling process in foaming.
7. The power-law model is used to describe the material behavior of the bubble growth.

GOVERNING EQUATIONS

Mass conservation for the melt

The continuity equation of a melt in a spherical coordinate system is given by eq. (2):

$$\frac{1}{r^2}\frac{\partial}{\partial t}\left(r^2 v_r\right) + \frac{1}{r\sin\theta}\frac{\partial}{\partial\theta}(v_\theta \sin\theta) + \frac{1}{r\sin\theta}\frac{\partial v_\varphi}{\partial\varphi} = 0 \tag{2}$$

where v_r is the radial velocity, v_θ is the velocity in the θ direction, and v_ϕ is the velocity in the ϕ direction, where θ and ϕ are coordinates in spherical coordinate system.

In a spherically symmetric expansion, $v_\theta = v_\phi = 0$, the continuity equation of melt yields the following form:

$$\frac{\partial v_r}{2v_r} = -\frac{2\partial r}{r} \tag{3}$$

The melt velocity at the bubble surface where $r = R$ is as follows:

$$v_R = \frac{dR}{dt} = \dot{R} \tag{4}$$

where v_R is the melt velocity at the bubble surface and $\dot{R}$ is the growth rate of the bubble and R is the radius of the bubble.

With the integration of eq. (3) and substitution of eq. (4) into the integral equation as a boundary condition, eq. (3) becomes

$$v_r = \frac{\dot{R}R^2}{r^2} \tag{5}$$

Momentum conservation for the melt

The conservation of momentum for the melt in the radial direction is given by eq. (6):

$$\rho\left(\frac{\partial v_r}{\partial t} + v_r\frac{\partial v_r}{\partial r}\right) = -\frac{\partial P}{\partial r} + \frac{1}{r^2}\frac{\partial}{\partial r}\left(r^2\tau_{rr}\right) - \frac{\tau_{\theta\theta} + \tau_{\phi\phi}}{r} \tag{6}$$

where ρ is the melt density, P is the pressure in the melt, and τ_{rr} and $\tau_{\theta\theta}$ are the normal stress in the radial and tangential directions, respectively.

The inertial term in the momentum equation is neglected as the melt is highly viscous and the Reynolds number is small enough. As the computational domain is spherical symmetry, this assumption leads to $\tau_{\theta\theta} = \tau_{\phi\phi}$, where $\tau_{\phi\phi}$ is the normal stress in the tangential direction of z-axial cross section. Hence, the differential of momentum conservation reduces to the following form:

$$-\frac{\partial P}{\partial r}+\frac{\partial \tau_{rr}}{\partial r}+2\left(\frac{\tau_{rr}-\tau_{\theta\theta}}{r}\right)=0 \tag{7}$$

Laplace's equation in the radial direction is as follows:

$$P_g - P_f + \tau_{p,rr}(R) - \tau_{g,rr}(R) = \sigma\left(\frac{1}{R_1}+\frac{1}{R_2}\right) \tag{8}$$

where $\tau_{p,rr}(R)$ is the normal stress of the polymer in the radial direction at the bubble surface, $\tau_{g,rr}(R)$ is the normal stress of the gas in the radial direction at the bubble surface, σ is the surface tension coefficient, and R_1 and R_2 are the principal radii of curvature.

The gas stress is close to zero and $R_1 = R_2$ in the sphere; consequently, Laplace's equation is reduced to eq. (9):

$$-P_f + \tau_{rr}(R) = -P_g + \frac{2\sigma}{R} \tag{9}$$

When the momentum conservation equation along the radial direction from the bubble surface R to the outer boundary of the cell S is integrated and eq. (9) is substituted into the integral momentum conservation equation at the bubble interface, the momentum conservation equation becomes:

$$P_g - \frac{2\sigma}{R} - P_f + 2\int_R^S \frac{\tau_{rr}-\tau_{\theta\theta}}{r}dr = 0 \tag{10}$$

Mass conservation for the gas in the melt and in the bubble

The gas diffusion from liquids to the bubble obeys the advection–diffusion equation:

$$\frac{\partial c}{\partial t}+v_r\frac{\partial c}{\partial r}=\frac{D}{r^2}\frac{\partial}{\partial r}\left(r^2\frac{\partial c}{\partial r}\right) \tag{11}$$

where D is the diffusion coefficient.

The mass conservation of the gas in the melt and in the bubble requires that the rate of mass added to the bubble is equal to the rate of mass diffusing through the bubble surface, as shown in eq. (12):

$$\frac{dm}{dt}=4\pi R^2 D\left.\frac{\partial c}{\partial r}\right|_{r=R} \tag{12}$$

where m is the number of moles of the gas in the bubble.

As the gas in the bubble is an ideal gas, the ideal gas equation is obeyed:

$$P_g V = mR_g T \tag{13}$$

where V is the bubble volume, R_g is the gas constant, and T is the gas temperature.

Equation (12) can be written as follows with eq. (13) put into.

$$\frac{d}{dt}\left(\frac{4\pi}{3}\frac{P_g R^3}{R_g T}\right)=4\pi R^2 D\left.\frac{\partial c}{\partial r}\right|_{r=R} \tag{14}$$

Truncated power-law equation

In this study, we used the truncated power-law model[10] to describe the rheology of the polymer, which is expressed in eqs. (15) and (16):

$$\boldsymbol{\tau} = 2\eta\mathbf{D} \tag{15}$$

$$\begin{cases} \eta = \eta_0 & \dot{\gamma} \le \dot{\gamma}_0 \\ \eta = \eta_0 \dot{\gamma}^{n-1} & \dot{\gamma} \ge \dot{\gamma}_0 \end{cases} \tag{16}$$

where $\boldsymbol{\tau}$ is the stress tensor, $\mathbf{D}$ is deformation rate tensor, η is the dynamic viscosity of the melt, η_0 is the zero-shear viscosity of the melt, n is the power-law index, $\dot{\gamma}_0$ is critical shear rate, and $\dot{\gamma}$ is the shear rate, which is expressed as follows:

$$\dot{\gamma}\sqrt{\frac{1}{2}\mathbf{II}_\Delta} \tag{17}$$

where $\mathbf{II}_\Delta$ is the second scalar invariant of the strain rate tensor, which is defined as

$$\begin{aligned}\frac{1}{2}\mathbf{II}_\Delta = 2\Bigg[&\left(\frac{\partial v_r}{\partial r}\right)^2+\left(\frac{1}{r}\frac{\partial v_\theta}{\partial\theta}+\frac{v_r}{r}\right)^2\\&+\left(\frac{1}{r\sin\theta}\frac{\partial v_\varphi}{\partial\varphi}+\frac{v_r}{r}+\frac{v_\theta\cot\theta}{r}\right)^2\Bigg]+\left[r\frac{\partial}{\partial r}\left(\frac{v_\theta}{r}\right)+\frac{1}{r}\frac{\partial v_r}{\partial\theta}\right]^2\\&+\left[\frac{\sin\theta}{r}\frac{\partial}{\partial\theta}\left(\frac{v_\varphi}{\sin\theta}\right)+\frac{1}{r\sin\theta}\frac{\partial v_\theta}{\partial\varphi}\right]^2\\&+\left[\frac{1}{r\sin\theta}\frac{\partial v_r}{\partial\varphi}+\frac{\partial}{\partial r}\left(\frac{v_\varphi}{r}\right)\right]^2\end{aligned} \tag{18}$$

Because of the spherically symmetric assumption, eq. (18) can be reduced to

TABLE I
Material and Process Parameters for the Low Density Polyethylene-Nitrogen System in Bubble Expansion[8,12,15]

Initial bubble radius	$R_0 = 1$ μm
Radius of the analysis region	$S_0 = 20$ μm
Diffusion coefficient	$D = 4.26 \times 10^{-9}$ m^2/s
Solubility coefficient	$K_H = 3.61 \times 10^{-5}$ mol N^{-1} m^{-1}
Surface tension and critical cluster	$\sigma = 11.5 \times 10^{-3}$ N/m
Loading pressure	$P_{g0} = 1.11 \times 10^7$ Pa
Ambient pressure	$P_f = 1.01 \times 10^5$ Pa
Temperature	$T = 423.8$ K
Zero-shear viscosity	$\eta_0 = 4.90 \times 10^4$ N s m^{-2}
Gas constant	$R_g = 8.31444$ J K^{-1} mol^{-1}
Power-law index	$n = 0.57$

$$\frac{1}{2}\mathbf{II}_\Delta = 2\left[\left(\frac{\partial v_r}{\partial r}\right)^2 + \left(\frac{v_r}{r}\right)^2\right] \tag{19}$$

NUMERICAL PROCEDURE

Finite element formulation

The Galerkin weighted residual method was adopted to discretize the convective–diffusion equation, where the weighted function was taken in the same form as the interpretation function. Equation (20) is the discretized convective–diffusion equation at the elemental level:

$$\sum_j \int_{-1}^{1} \left[\frac{\partial c}{\partial t} + v_r\frac{\partial c}{\partial r} - \frac{D}{r^2}\frac{\partial}{\partial r}\left(r^2\frac{\partial c}{\partial r}\right)\right] N_i d\xi = 0 \tag{20}$$

$$N_i = \frac{1}{2}(1 + \xi_i\xi)(i = 1, 2) \tag{21}$$

where j is the number of finite elements, N_i is the interpolation function of the dissolved gas concentration, ξ is the local coordinate in each element, and ξ_i is the local coordinate values of the nodes.

After Green–Gauss transformation, eq. (22) is obtained as the following weak form:

$$\sum_j \int_{-1}^{1} \frac{\partial c}{\partial t} N_i dr + \int_{-1}^{1} \left(\frac{R^2\dot{R}}{r^2} - \frac{D}{r}\right)\frac{\partial c}{\partial r} N_i d\xi = \sum_l D\frac{\partial c}{\partial r}\bigg|_{\xi=-1} \tag{22}$$

where l is the number of elements on the boundary of computational domain.

As $\partial c/\partial r = 0$ at the outer surface ($\xi = 1$) of the cell, only one item is left on the right-hand side of eq. (22).

The global stiffness matrix equation of the convective–diffusion equation, eq. (23), for all the elements is assembled after the elemental stiffness matrix is calculated according to the nodes superposition principle:

$$\mathbf{A}\dot{c} + \mathbf{B}c = \mathbf{F} \tag{23}$$

where $\dot{c}$ is the time rate of dissolved gas concentration, **A** is the transient matrix, **B** is the stiffness matrix, and **F** is the coefficient matrix. One can obtain the concentration of dissolved gas by solving the global stiffness matrix equation of eq. (23) using the Gauss–Seidel iteration method.[22]

As mentioned in the Model Description and Assumptions section, the gas concentration at the bubble surface obeys Henry's law, and no gas diffuses to the surroundings at the outer boundary of the melt. Essential and natural boundary conditions are applied on the inner and outer boundaries of the cell separately.

Solution method

At each time step, with the initial value of R and P_g, eqs. (10) and (14) were solved simultaneously to obtain the values of R and P_g. Then, eq. (23) was solved, and time was discretized with implicit difference. The nodes near the bubble surface moved faster than those far from the interface, and the grids near the bubble surface deformed seriously during the process. The grids were remeshed to assure the accuracy of the calculation after each time step. The values of the parameters used in the computation program are listed in Table I.[8,12,15]

RESULTS AND DISCUSSION

Gas concentration profile in the melt

Figure 2 shows the gas concentration at both the bubble surface and outside of the melt. The gas

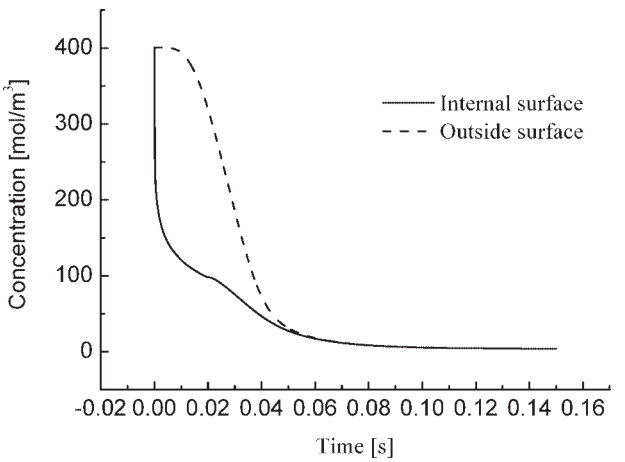

Figure 2 Gas concentration at the bubble internal surface and outside surface.

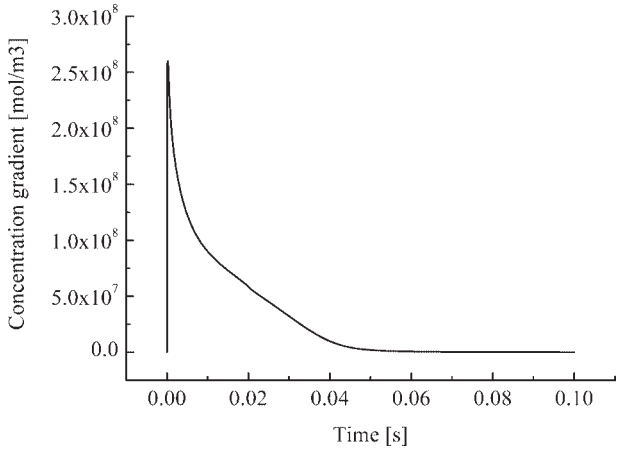

Figure 3 Gas concentration gradient at the bubble internal surface.

concentration at the bubble surface dropped greatly, whereas the concentration at the edge of the cell changed little during the first 0.01 s. This was because P_g changed from a high initial gas pressure at the supersaturated state to a relatively low ambient pressure. According to the Henry's law, the concentration at the bubble surface dropped consequently; this resulted in a great concentration gradient at the bubble surface, as shown in Figure 3. The concentration gradient was the driving force of gas diffusion in the melt, so gas diffusion occurred earlier near the bubble surface than at the edge of the cell. As the bubble grew, the bubble pressure decreased and finally approached ambient pressure. The bubble growth stopped when the gas concentration in the melt was equal everywhere and the pressure difference was close to zero.

Variability of the bubble radius and bubble pressure with time

At the beginning of bubble growth, the pressure of the melt dropped from a relatively high initial pressure to ambient pressure; meanwhile, the pressure

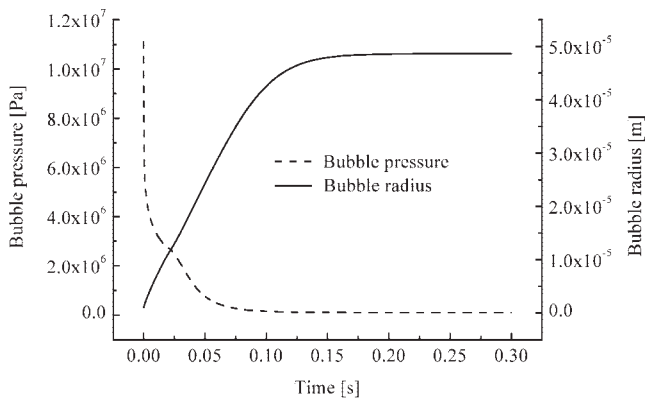

Figure 4 Variability of the bubble radius and bubble pressure with time.

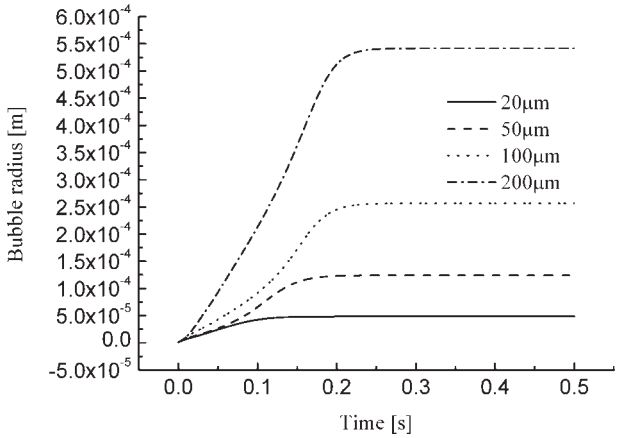

Figure 5 Effect of the outer radius of the cell on bubble growth.

inside the bubble dropped rapidly, too. A pressure difference was formed between the bubble pressure and the ambient pressure, and the bubble started to grow. Figure 4 shows the variation of the bubble radius and bubble pressure with time. The bubble pressure reached equilibrium at about 0.1 s, but the bubble radius reached its final value later. During the initial stage of bubble growth, the bubble pressure decreased rapidly, and the high pressure difference was the main driver for bubble growth. As bubble growth continued, a differential concentration of the gas formed in the melt, and the gas diffused into the bubble. When the pressure difference decreased to zero, the gas concentration in the melt had not achieved equilibrium, and the bubble continued to grow. So we drew the conclusion that the pressure difference was the main driver for bubble growth at the early stage of bubble growth, but as the pressure difference decreased, the gas diffused from the melt into the bubble continuously, and it became the main force of bubble growth.

Effect of the outer radius of the cell on bubble growth

The simulation described in this section used the same initial bubble radius ($R_0 = 1$ μm) but a different initial outer radius (S_0) of the cell, and the other parameters were the same as those listed in Table I. Figure 5 gives the effect of the outer radius of the cell on bubble growth. The final bubble radius increased as S_0 increased. Obviously, the increase in S_0 resulted in a large volume of liquids that surrounded the bubble; this led to an increase in the total mass of dissolved gas in the influence cell. As a result, more gas was available to diffuse from the melt into the bubble. So it took more time for the bubble with a larger outer radius to reach its final size, and the bubble with a smaller outer radius reached its equilibrium faster.

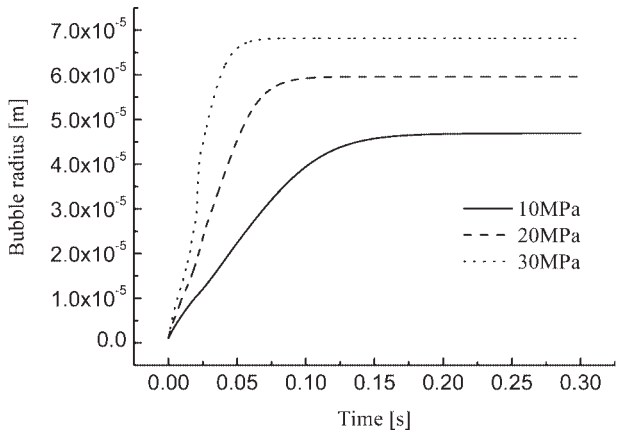

Figure 6 Effect of the initial pressure on bubble growth.

Effect of the initial gas pressure on bubble growth

Bubble growth was controlled by both the pressure difference between the bubble pressure and ambient pressure and gas diffusion. The gas diffusion in the melt was of great importance for bubble growth. The process of gas diffusion was mainly controlled by the diffusion coefficient. When the temperature and the pressure of the melt changed, the diffusion coefficient changed with them. The relation between the diffusion coefficient at different temperatures and gas pressure is shown in eq. (24):[23]

$$D = D_0\left(\frac{P_0}{P_g}\right)\left(\frac{T}{T_0}\right)^{n_t} \tag{24}$$

where D is the diffusion coefficient at any temperature T and P_g, D_0 is the diffusion coefficient at temperature T_0 and pressure P_0, and n_t is the temperature index.

Actually, the gas diffusion coefficient was in inverse proportion to the pressure. When the initial pressure in the melt increased, the gas diffusion coefficient decreased. The decrease in the diffusion coefficient led to less gas diffusing into the bubble; this went against bubble growth. On the other hand, when the initial pressure in the melt increased, the pressure difference between the bubble pressure and ambient pressure increased, which was good for bubble growth. Figure 6 shows the effect of the initial gas pressure on bubble growth. As shown, the final bubble radius increased with increasing initial gas pressure. Although the gas diffusion coefficient decreased as the gas pressure increased, the gas concentration in the melt increased. On the whole, more gas was available for diffusion. So as the initial gas pressure increased, more gas resolved in the melt, and the pressure difference increased; this resulted in a larger final bubble radius.

Effect of the temperature on bubble growth

Both the viscosity and diffusion coefficient changed as the temperature varied. The change in the diffusion coefficient with temperature obeyed eq. (24), and the change in viscosity with temperature obeyed the Arrhenius equation, which is written as follows:[24]

$$\eta = \eta_0 \exp\left[\frac{E_r(T_0 - T)}{RT_0T}\right] \tag{25}$$

where E_r is the viscous flow activation energy.

Figure 7 shows that the bubble grew faster as the liquid temperature increased. When the liquid temperature increased, the zero-shear viscosity of the liquids decreased, and the stress of the liquids decreased; this acted as resistance to bubble growth. The diffusion coefficient increased, too, as the temperature increased. So the bubble grew faster at a higher liquid temperature. Meanwhile, P_g dropped faster, too. The pressure difference between the gas pressure and ambient pressure, which was one of the driving forces to bubble growth, dropped faster as a result. On the whole, the final bubble radius was a little larger when the foaming process occurred at a higher liquid temperature.

Effect of the polymer rheology on bubble growth

In this study, we used Newtonian and truncated power-law constitutive equations to describe the rheology of liquids. Under isothermal conditions, the viscosity of a Newtonian liquid remains constant during the whole bubble growing process. However, for a truncated power-law liquid, the viscosity decreases as the shear rate increases for the part of melt that is described by the power-law model. In the case of the truncated power-law liquid, as the bubble grows, the shear rate increases, more melt obeys the power-law model, and its viscosity

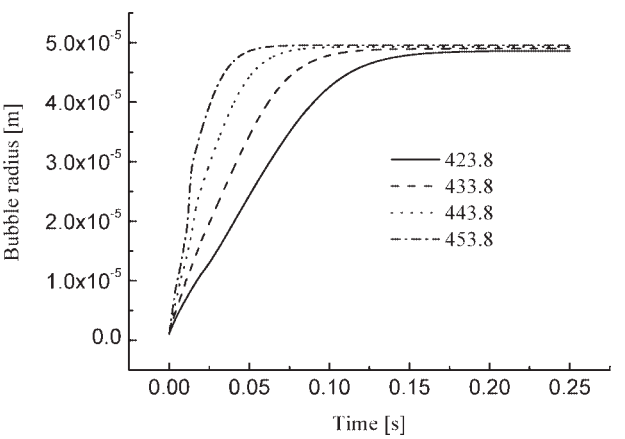

Figure 7 Effect of the temperature on bubble growth.

decreases at the same time. Figure 8 shows bubble growth with different power-law indices. As the power-law index increased, shear thinning became less obvious, but the bubble grew faster. When the power-law index reached 1.0, the polymer became a Newtonian liquid, and the bubble obtained a larger final radius. As shown in Figure 8, the bubble growth rate changed with different power-law indices, but the final radius was almost the same. So the power-law index had more influence on the bubble growth rate than the final bubble radius.

Comparison with other works

It was necessary to compare the results of our work with that of others. Mao et al.[25] carried out a simulation of bubble growth with a modified influence volume approach. They defined two distinct stages of bubble growth, namely, the free- and limited expansion stages. In the earlier free-expansion stage, both bubble nucleation and growth occurred, and the bubble pressure dropped substantially from an initially high pressure in the supersaturated state, whereas the dissolved gas concentration changed very little. The second stage was termed the *limited expansion stage* and accounted for bubble growth in the late stages of foam evolution, when the pressure changes became small, but the dissolved gas concentration dropped significantly.

With the parameters taken by Mao et al.,[25] bubble growth simulation was executed with our simulation codes. As shown in Figure 9, the final bubble radius was almost the same, and the growth tendency was similar. As nucleation was not considered in our study, bubble growth started at a given initial radius, so bubble growth started earlier in our study than in Mao et al.'s. In Mao et al.'s simulation, as mentioned, the dissolved gas concentrations in the liquids were approximately constants, and the difference between the bubble pressure and the ambient pressure was the mechanism that dictated initial bubble growth. However, in our study, the bubble pressure dropped dramatically from the very beginning, and the dissolved gas concentration dropped with it. Not only the pressure difference but also the concentration gradient were the bubble growth driving forces. Thus, the bubble grew faster at the initial stage and reached its finial radius in a shorter time in our study. With the effect of nucleation on bubble growth taken into consideration, the results in our work agree well with those of Mao et al.

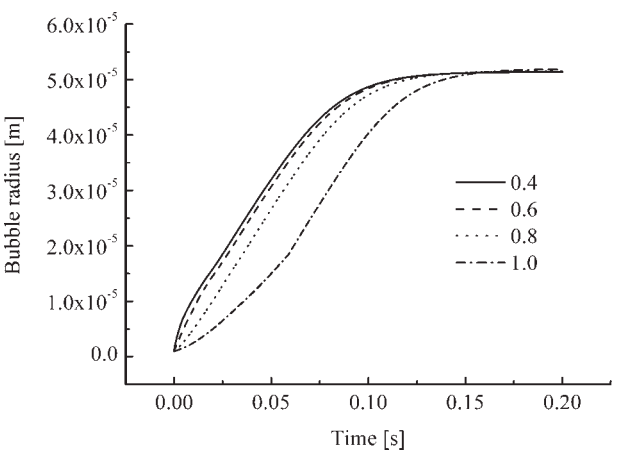

Figure 8 Effect of the power-law index on bubble growth.

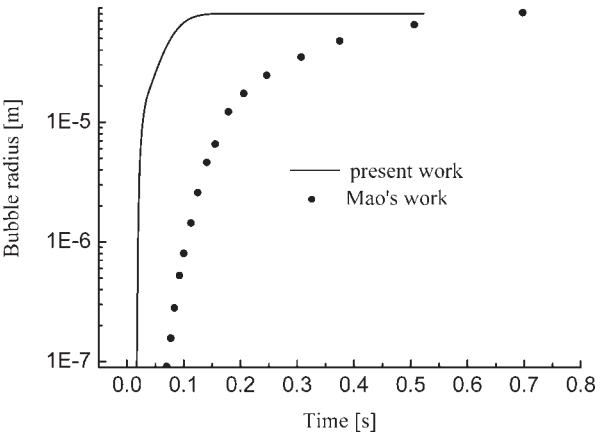

Figure 9 Comparison with the simulation data of Mao et al.[25]

CONCLUSIONS

A finite element method (FEM) simulation of a spherical bubble growth process based on momentum and mass control is presented. Computer code was written to solve the equations governing bubble growth. The numerical results could predict the instantaneous bubble size, bubble pressure, and gas concentration profile in liquids. A truncated power-law model was adopted to describe the rheology of liquids. The results show that the bubble reached a larger final radius with larger cell volume. With the influence of the pressure on the diffusion coefficient ignored, the bubble achieved a larger final radius under a higher gas pressure. Otherwise, smaller bubbles were obtained when the gas pressure increased. The bubble grew faster but reached a smaller final bubble radius at higher liquid temperatures. The effect of rheology on bubble growth indicated that the bubble achieved a larger final radius in Newtonian liquids than in power-law liquids, and the bubble grew faster as the power index decreased. Finally, we compared our results to that of others using the same parameters but different numerical methods, and the results agreed well.

References

1. Beydokhti, K. K.; Behravesh, A. H.; Azdast, T. Iranian Polym J 2006, 15, 555.
2. Arefmanesh, A.; Advani, S. G.; Michaelides, E. E. Int J Heat Mass Transfer 1992, 35, 1711.
3. Greco, A.; Maffezzoli, A.; Manni, O. Polym Degrad Stab 2005, 90, 256.
4. Koehler, S. A.; Hilgenfeldt, S.; Stone, H. A. J Colloid Interface Sci 2004, 276, 420.
5. Tai, H.-J. J Polym Res 2005, 12, 457.
6. Arefmanesh, A.; Advani, S. G. Polym Eng Sci 1995, 35, 252.
7. Frank, X.; Dietrich, N.; Wu, J.; Barraud, R.; Li, H. Z. Chem Eng Sci 2007, 62, 7090.
8. Venerus, D. C.; Yala, N.; Bernstein, B. J Non-Newtonian Fluid Mech 1998, 75, 55.
9. Lastochkin, D.; Favelukis, M. Chem Eng J 1998, 69, 21.
10. Favelukis, M.; Albalak, R. J. Chem Eng J 1996, 63, 149.
11. Shaft, M. A.; Joshi, K.; Flumerfelt, R. W. Chem Eng Sci 1997, 52, 635.
12. Joshi, K.; Lee, J. G.; Shafi, M. A.; Flumerfelt, R. W. J Appl Polym Sci 1998, 67, 1353.
13. Favelukis, M. Polym Eng Sci 2004, 44, 1900.
14. Amon, M.; Denson, C. D. Polym Eng Sci 1984, 24, 1028.
15. Feng, J. J. J Rheol 2004, 48, 439.
16. Koopmans, R. J.; den Doelder, J. C. F.; Paquet, A. N. Adv Mater 2000, 12, 1873.
17. Kim, K. Y.; Kang, S. L.; Kwak, H.-K. Polym Eng Sci 2004, 44, 1890.
18. Favelukis, M.; Zhang, Z.; Pai, V. Polym Eng Sci 2000, 40, 1350.
19. Bruchon, J.; Fortin, A.; Bousmina, M.; Benmoussa, K. Int J Numer Meth Fluids 2007, 54, 73.
20. Otsuki, Y.; Kanai, T. Polym Eng Sci 2005, 45, 1277.
21. Taki, K. Chem Eng Sci 2008, 63, 3643.
22. Verwer, J. G. J Sci Comput 1994, 15, 1243.
23. Poling, B.; Prausnitz, J.; O' Connell, J. The Properties of Gases and Liquids; McGraw-Hill: New York, 2000.
24. Schramm, G. A Practical Approach to Rheology and Rheometry; Gebrueder HAAKE: Karlsruhe, Federal Republic of Germany, 1994.
25. Mao, D.; Edwards, J. R.; Harvey, A. Chem Eng Sci 2006, 61, 1836.